Seismic Response Analysis of the Planar Rocking Frame

Elias G. Dimitrakopoulos[1] and Anastasios I. Giouvanidis[2]

Abstract: Unlike conventional seismic design, the columns of a rocking frame are designed to uplift and pivot during earthquake excitation. This paper investigates, analytically and numerically, the seismic response of a rocking frame with columns unequal in height (asymmetric), which are either freestanding or hybrid, i.e., enhanced with supplemental damping and recentering capacity. The paper establishes the equations of motion following the principles of analytical dynamics. Throughout the study, the deformation of the structural members is considered negligible. The analysis considers both pulse-type and non-pulse-type (historic) ground motions. It shows that the effect of asymmetry on the seismic stability of the rocking frame is marginal compared with the symmetric configuration, despite the very different kinematics of the corresponding rocking mechanisms. In contrast, the seismic stability of the hybrid rocking frame is very sensitive to fracture elongation of the supplemental restoring (tendons) and damping devices. The results confirm the high-performance seismic behavior of the planar rocking frame, thus illustrating its potential as an alternative seismic design paradigm. **DOI: 10.1061/(ASCE)EM.1943-7889.0000939.**

Author keywords: Rocking frame; Seismic resistant structures; Analytical dynamics; Prefabricated bridges; Seismic isolation; Overturning; Self-centering.

Introduction

The idea of allowing columns to uplift and pivot (i.e., rocking behavior) as a means of seismic isolation during a strong earthquake event is not new. Ancient monuments survived millennia within earthquake-prone regions mainly owing to the development of rocking behavior (Papaloizou and Komodromos 2009, 2012; Psycharis et al. 2013). Focusing on contemporary structures, existing rocking bridges in New Zealand, e.g., the Rangitikei Railway Bridge and the Deadman's Point Bridge at Cromwell (Priestley et al. 1996; Skinner et al. 1980), and novel research studies (Housner 1963; Kelly and Tsztoo 1977), date back to the 1960s and 70s. This alternative seismic design hinges on diminishing structural deformation (and therefore damage) by allowing rigid body movements of structural segments around predefined interfaces, and it is currently resurging (Aaleti and Sritharan 2009; Acikgoz and DeJong 2014; Antonellis and Panagiotou 2013; Dimitrakopoulos and DeJong 2012b; Kafle et al. 2011; Voyagaki et al. 2013).

The beneficial isolation effect of rocking has been confirmed experimentally for a variety of structural configurations, including buildings [e.g., posttensioned precast wall systems (Aaleti and Sritharan 2009) or self-centering steel-braced frames (Eatherton et al. 2014)], as well as bridges [e.g., an A-shaped (pure) rocking pier (Chen et al. 2006), a single rocking pier with additional dissipaters (Solberg et al. 2009), or a two-column rocking bridge bent with central posttensioned tendons (Cheng 2008)]. The addition of adequate self-centering capacity (central tendons) reduces remarkably the residual displacements/deformations, without altering significantly the peak response displacements of the rocking piers (Sakai and Mahin 2004). Further, the addition of energy dissipation limits the amplitude of rocking (DeJong and Dimitrakopoulos 2014; Dimitrakopoulos and DeJong 2012a, b, 2013; Roh and Reinhorn 2010), and the dissipaters could be replaceable and of low cost (Pollino and Bruneau 2007). The combination of supplemental damping and additional recentering devices leads to hybrid-rocking systems. Such hybrid-rocking bridges have been proposed as high-performance systems that could survive major earthquakes without significant damage (Palermo et al. 2005, 2007; Marriott et al. 2009; Kam et al. 2010; and among others).

The structural configuration of the rocking frame (Fig. 1) seems to be a promising combination of the merits of the precast construction method (Pang et al. 2008; Wacker et al. 2005; and references therein), with the benefits of rocking isolation. Following the seminal work of Priestley and Tao (1993) for buildings, Mander and Cheng (1997) proposed the rocking bridge bent (i.e., the rocking frame) as a *damage-avoidance design* for bridges. Makris and Vassiliou (2012) revisited the seismic response of the rocking frame. That study illustrated the direct equivalence between the response of the symmetric rocking frame and the rocking block, and investigated numerically its seismic stability within the context of a potential bridge application. Importantly, the Makris and Vassiliou (2014) work proved that the rocking frame is more stable, the more top-heavy it is. Recently, DeJong and Dimitrakopoulos (2014) coined a methodology to derive an exact or approximate equivalence between complicated rocking structures (e.g., the rocking wall, the rocking frame, and the rocking arch) and the archetypal rocking block.

The present study extends previous work on the rocking frame (DeJong and Dimitrakopoulos 2014; Dimitrakopoulos et al. 2013; Makris and Vassiliou 2012) examining a frame that is (1) hybrid (enhanced with additional energy dissipation and recentering capacity) and/or (2) not symmetric. As the study shows, the symmetric rocking frame represents a very limited case from a mechanics perspective, because the slightest deviation from the (perfect) symmetric geometry triggers an entirely different kinematic

[1]Assistant Professor, Dept. of Civil and Environmental Engineering, Hong Kong Univ. of Science and Technology, Kowloon Bay, Hong Kong (corresponding author). E-mail: ilias@ust.hk

[2]Postgraduate Student, Dept. of Civil and Environmental Engineering, Hong Kong Univ. of Science and Technology, Kowloon Bay, Hong Kong. E-mail: agiouvanidis@ust.hk

Note. This manuscript was submitted on June 12, 2014; approved on January 26, 2015; published online on April 15, 2015. Discussion period open until September 15, 2015; separate discussions must be submitted for individual papers. This paper is part of the ***Journal of Engineering Mechanics***, © ASCE, ISSN 0733-9399/04015003(13)/$25.00.

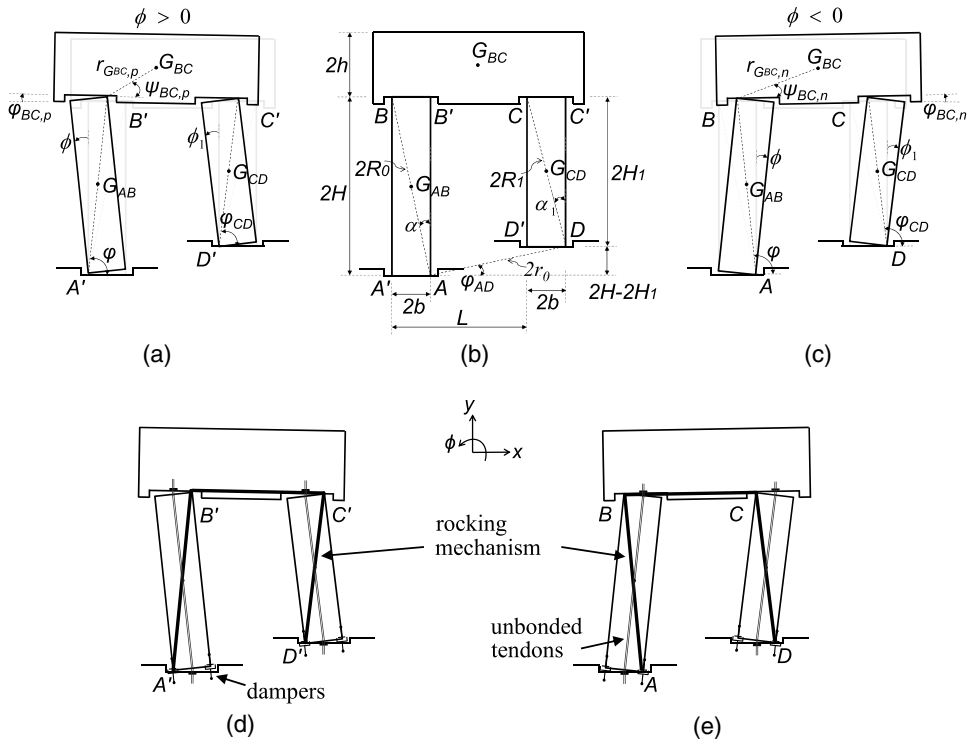

Fig. 1. Examined rocking frame: (a) during counterclockwise rotation; (b) at rest position; (c) during clockwise rotation and the rocking mechanisms for (d) counterclockwise; (e) clockwise rotation

mechanism. This asymmetric mechanism has not been studied before, although it is imperative to do so if the symmetric rocking frame is to be adopted as a realistic seismic design paradigm. Similarly, the characteristics of the supplemental damping and restoring devices (and primarily their ultimate fracture elongation) might dominate the seismic response (Dimitrakopoulos and DeJong 2012a) and should, therefore, be carefully studied and designed. This study is motivated by the need to assess the relative importance of two basic design aspects: (1) the characteristics of the supplemental damping and restoring devices, and (2) the asymmetry of the frame geometry, to pave the way for future (novel) applications of the rocking frame as an alternative seismic design solution.

Analytical Modeling of the Asymmetric Hybrid Rocking Frame

This section builds on previous research on the seismic response of the planar rocking frame (DeJong and Dimitrakopoulos 2014; Dimitrakopoulos et al. 2013; Makris and Vassiliou 2012). The study focuses on structures designed to use planar rocking, as opposed to structures that (accidentally) happened to rock. Rocking is assumed to be confined within a desired plane, and accidental three-dimensional rocking is ignored. However, for the general case of nonplanar motion of rocking structures the reader is referred to Chatzis and Smyth (2012) and Zulli et al. (2012).

Consider the (hybrid) rocking frame enhanced with central unbonded tendons and viscous dampers at the bottom of the piers (Fig. 1). To offer insight on the effect of the supplemental damping and the additional stiffness on the seismic stability of the rocking frame in a general way without considering the detailed behavior of specific supplemental devices, this study assumes (as a first approach) that the mechanical behavior of the tendons is that of ideal springs, and the behavior of the dampers is that of ideal linear-elastic viscous dashpots. The two columns of the frame have different heights H_1 and H. Further, sliding at the contact surfaces is ignored. However, regarding the influence of sliding on rocking structures the reader is referred to Brogliato et al. (2012). Therefore, ignoring the deformation of the (three) members, this asymmetric hybrid rocking frame exhibits a three-block rocking mechanism (Fig. 1). The equations offered in the present section also cover the symmetric rocking frame, freestanding or hybrid, as a special case ($H_1 = H$).

Kinematics

Fig. 1 illustrates the assumed three-block mechanism for clockwise (negative: subscript n) and counterclockwise (positive: subscript p) rotations and the pertinent pivot points A, B, C, D and A′, B′, C′, D′ accordingly. Because of unequal heights, the two columns exhibit different rocking rotations and the connecting beam, apart from a rigid-body translation, also sustains rigid-body rotation (Fig. 1).

The kinematics of the three-block mechanism is far from trivial and has been the subject of extensive research in the literature of linkages, machines, and mechanisms under the term *four-bar linkage* [see for instance Ceccarelli (2007), Freudenstein (2010), and references therein]. The following discussion is confined to the needs of the present study. The three-block mechanism of Fig. 1 can be captured with a single generalized coordinate, selected to be the angle φ of segment AB with respect to the x-axis. The pertinent rocking amplitude is simply the rotation ϕ with respect to the initial position: $\phi = \varphi - \varphi_{0,p}$ for the counterclockwise (positive) rotation and $\phi = \varphi - \varphi_{0,n}$ for the clockwise (negative) rotation (Fig. 1).

The orientation of the bars BC and CD, with respect to the positive x-axis can be written as a function of the generalized coordinate and known geometry

$$\varphi_{\mathrm{BC}}(\varphi) = \arctan\left[\frac{-R_0\sin\varphi + r_0\sin\varphi_{\mathrm{AD}} + R_1\sin\varphi_{\mathrm{CD}}(\varphi)}{-R_0\cos\varphi + r_0\cos\varphi_{\mathrm{AD}} + R_1\cos\varphi_{\mathrm{CD}}(\varphi)}\right]$$
$$\varphi_{\mathrm{CD}}(\varphi) = \arctan\left(\frac{R_0\sin\varphi - r_0\sin\varphi_{\mathrm{AD}}}{R_0\cos\varphi - r_0\cos\varphi_{\mathrm{AD}}}\right) - \arccos\left[\frac{\mathrm{BD}^2(\varphi) + 4R_1^2 - L^2}{4R_1\cdot\mathrm{BD}(\varphi)}\right] \quad (1)$$

where R_0, R_1 and r_0 = half-lengths of blocks AB, CD, and AD respectively; and length BD is given as (Fig. 1)

$$\mathrm{BD}^2(\varphi) = (2R_0)^2 + (2r_0)^2 - 8R_0r_0\cos(\varphi - \varphi_{\mathrm{AD}}) \quad (2)$$

Differentiating the rotations with respect to time yields the corresponding angular velocities

$$\dot\varphi_{\mathrm{BC}}(\varphi,\dot\varphi) = \frac{\partial\varphi_{\mathrm{BC}}}{\partial\varphi}\dot\varphi = \partial_\varphi\varphi_{\mathrm{BC}}(\varphi)\cdot\dot\varphi,$$
$$\dot\varphi_{\mathrm{CD}}(\varphi,\dot\varphi) = \frac{\partial\varphi_{\mathrm{CD}}}{\partial\varphi}\dot\varphi = \partial_\varphi\varphi_{\mathrm{CD}}(\varphi)\cdot\dot\varphi \quad (3)$$

where $\dot\varphi$ = angular velocity of the member AB (upper dot denotes differentiation with respect to time); and ∂_φ = partial derivative with respect to the (subscript) φ. Similarly, the second derivatives with respect to φ are defined as

$$\frac{\partial^2\varphi_{\mathrm{BC}}}{\partial\varphi^2} = \partial^2_{\varphi\varphi}\varphi_{\mathrm{BC}}(\varphi), \qquad \frac{\partial^2\varphi_{\mathrm{CD}}}{\partial\varphi^2} = \partial^2_{\varphi\varphi}\varphi_{\mathrm{CD}}(\varphi) \quad (4)$$

Further, the displacements of the centers of mass G_{AB}, G_{BC}, G_{CD} of the frame members are (Fig. 1)

$$x^G_{\mathrm{AB}}(\varphi) = 2b + R_0\cos\varphi$$
$$x^G_{\mathrm{BC}}(\varphi) = 2b + 2R_0\cos\varphi + r^G_{\mathrm{BC}}\cos[\varphi_{\mathrm{BC}}(\varphi) + \psi_{\mathrm{BC}}]$$
$$x^G_{\mathrm{CD}}(\varphi) = L + 2b + R_1\cos\varphi_{\mathrm{CD}}(\varphi)$$
$$y^G_{\mathrm{AB}}(\varphi) = R_0\sin\varphi$$
$$y^G_{\mathrm{BC}}(\varphi) = 2R_0\sin\varphi + r^G_{\mathrm{BC}}\sin[\varphi_{\mathrm{BC}}(\varphi) + \psi_{\mathrm{BC}}]$$
$$y^G_{\mathrm{CD}}(\varphi) = 2H - 2H_1 + R_1\sin\varphi_{\mathrm{CD}}(\varphi) \quad (5)$$

In Eq. (5) and throughout the present study, the distance r^G_{BC} from the pivot points B or B′ to the center of mass G_{BC} and the angle ψ_{BC} take different values with respect to the sign of rotation, and they are defined from the geometry of the frame (Fig. 1). Differentiating Eq. (5), the velocities of the three frame members are determined.

Equation of Motion during Rocking

The equation of motion for the rocking mechanism of Fig. 1 can be derived using Lagrange's equation:

$$\frac{d}{dt}\left(\frac{\partial T}{\partial\dot\varphi}\right) - \frac{\partial T}{\partial\varphi} + \frac{\partial V}{\partial\varphi} = Q \quad (6)$$

where T = kinetic energy; V = potential energy; Q = generalized force; and φ = generalized coordinate that describes the rocking motion. The potential energy of the three-block mechanism can be expressed as:

$$V = V_{fr} + V_{\mathrm{tend}} \quad (7)$$

where V_{fr} = potential energy of the freestanding frame (due to the gravitational forces); and V_{tend} = additional potential energy due to the elongation of the tendons. It holds that

$$V_{fr} = g[(m_{\mathrm{AB}} + 2m_{\mathrm{BC}})R_0\sin\varphi + m_{\mathrm{BC}}r^G_{\mathrm{BC}}\sin(\varphi_{\mathrm{BC}} + \psi_{\mathrm{BC}}) + m_{\mathrm{CD}}(2H - 2H_1 + R_1\sin\varphi_{\mathrm{CD}})] \quad (8)$$

where m_{AB}, m_{BC}, and m_{CD} = masses of blocks AB, BC, and CD accordingly.

During rocking, each tendon deforms into three inclined segments with different slopes. The length of these (three) segments depends on the rocking rotation ϕ, and subsequently, so does the exact value of the strain energy. For small rotations however, the strain energy is approximately calculated from the net elongation of each tendon, equal to the sum of the elongations at the base and the top of each tendon, which is equivalent with assuming that the tendons remain straight. Hence

$$V_{\mathrm{tend}} = \frac{1}{2}k(\delta l_{\mathrm{A}} + \delta l_{\mathrm{B}})^2 + \frac{1}{2}k(\delta l_{\mathrm{C}} + \delta l_{\mathrm{D}})^2 \quad (9)$$

For the AB tendon, the elongations at the base δl_{A} and the top δl_{B} are

$$\delta l_{\mathrm{A}} = 2b\sin\left(\frac{\phi}{2}\right), \qquad \delta l_{\mathrm{B}} = 2b\sin\left(\frac{\phi + \varphi_{\mathrm{BC}}}{2}\right) \quad (10)$$

Similarly, for the CD tendon

$$\delta l_{\mathrm{D}} = 2b\sin\left(\frac{\phi_1}{2}\right), \qquad \delta l_{\mathrm{C}} = 2b\sin\left(\frac{\phi_1 + \varphi_{\mathrm{BC}}}{2}\right) \quad (11)$$

where

$$\phi = -\frac{\pi}{2} \pm \alpha + \varphi \quad \text{and} \quad \phi_1 = -\frac{\pi}{2} \pm \alpha_1 + \varphi_{\mathrm{CD}} \quad (12)$$

are the rocking rotations of the AB and CD column, respectively (Fig. 1). Further, $\alpha_1 = b/H_1$ = slenderness of the CD column (Fig. 1); and $k = EA/l$ = stiffness of the tendons, with E = Young's modulus, A = the cross-sectional area, and l = length of each tendon. For simplicity, the present study assumes the two tendons have the same stiffness. Again, assuming the supplemental tendons AB and CD are effectively straight (small rotations/deformations assumption), strains $\varepsilon_{\mathrm{AB}}$ and $\varepsilon_{\mathrm{CD}}$ are $\varepsilon_{\mathrm{AB}} = k(\delta l_{\mathrm{A}} + \delta l_{\mathrm{B}})/(EA)$ and $\varepsilon_{\mathrm{CD}} = k(\delta l_{\mathrm{C}} + \delta l_{\mathrm{D}})/(EA)$, respectively.

In Eq. (12), and throughout this paper, the upper of the two signs corresponds to counterclockwise (positive) rocking rotation, and the lower sign to clockwise (negative) rocking rotation. The strain energy expression of Eq. (9) can be simplified for small rotations as in Appendix I [Eq. (34)].

Ignoring the mass of the tendons and the dampers, the kinetic energy of the system is

$$T = \frac{1}{2}I_{\mathrm{AB}}\dot\varphi^2 + \frac{1}{2}I_{\mathrm{BC}}(\partial_\varphi\varphi_{\mathrm{BC}}\cdot\dot\varphi)^2 + \frac{1}{2}I_{\mathrm{CD}}(\partial_\varphi\varphi_{\mathrm{CD}}\cdot\dot\varphi)^2 + \frac{1}{2}m_{\mathrm{BC}}[(2R_0)^2 + 4R_0r^G_{\mathrm{BC}}\cos(\varphi - \varphi_{\mathrm{BC}} - \psi_{\mathrm{BC}})\partial_\varphi\varphi_{\mathrm{BC}}]\dot\varphi^2 \quad (13)$$

where I_{AB} mass moment of inertia of AB with respect to the pivot point A (or A′ depending on the rocking mechanism/rotation); and I_{BC} and I_{CD} = pertinent quantities for members BC and CD respectively.

The calculation of the virtual work of the nonconservative forces Q yields the generalized forces:

$$\delta W_{nc} = Q\delta\varphi \Rightarrow \delta W_G + \delta W_D = (Q_G + Q_D)\delta\varphi \quad (14)$$

where δW_G and δW_D correspond to the work done by the nonconservative forces (inertia and damping) (Oppenheim 1992). More specifically, the generalized inertia force Q_G is:

$$Q_G = -\{m_{AB}R_0 \sin\varphi + m_{CD}R_1 \sin\varphi_{CD}\partial_\varphi\varphi_{CD} + m_{BC}[2R_0 \sin\varphi + r^G_{BC}\sin(\varphi_{BC}+\psi_{BC})\partial_\varphi\varphi_{BC}]\}\ddot{u}_g \quad (15)$$

and the generalized damping force Q_D is

$$Q_D = -2Cb^2\{[1 \pm \sin(\alpha \pm \varphi)] + [1 \pm \sin(\alpha_1 \pm \varphi_{CD})]\partial_\varphi\varphi^2_{CD}\}\dot{\varphi} \quad (16)$$

where C = damping constant of the linear viscous dampers. Again, the upper sign holds for counterclockwise (positive) rotation, and the lower for clockwise (negative) rotation. After substituting into Lagrange's Eq. (6), the equation of motion can be written as

$$I_{nl}(\varphi)\ddot{\varphi} + J_{nl}(\varphi)\dot{\varphi}^2 + G_{nl}(\varphi)g + K_{nl}(\varphi) + D_{nl}(\varphi)\dot{\varphi} = B_{nl}(\varphi)\ddot{u}_g \quad (17)$$

Note that Eq. (17) is not equivalent with the equation of motion of the rocking block (DeJong and Dimitrakopoulos 2014), even if the additional terms due to the dampers and the tendons are neglected. The terms I_{nl}, J_{nl}, G_{nl}, B_{nl}, K_{nl}, and D_{nl} are nonlinear functions of the generalized coordinate and equal with:

$$\begin{aligned}
I_{nl}(\varphi) &= \{I_{AB} + I_{BC}(\partial_\varphi\varphi_{BC})^2 + I_{CD}(\partial_\varphi\varphi_{CD})^2 + 4m_{BC}R_0[R_0 + r^G_{BC}\cos(\varphi - \varphi_{BC} - \psi_{BC})\partial_\varphi\varphi_{BC}]\}\\
J_{nl}(\varphi) &= -\{I_{BC}\partial_\varphi\varphi_{BC}\partial^2_{\varphi\varphi}\varphi_{BC} + I_{CD}\partial_\varphi\varphi_{CD}\partial^2_{\varphi\varphi}\varphi_{CD} + 2m_{BC}R_0 r^G_{BC}[\cos(\varphi - \varphi_{BC} - \psi_{BC})\partial^2_{\varphi\varphi}\varphi_{BC} + \sin(\varphi - \varphi_{BC} - \psi_{BC})(1 - \partial_\varphi\varphi_{BC})\partial_\varphi\varphi_{BC}]\}\\
G_{nl}(\varphi) &= (m_{AB} + 2m_{BC})R_0\cos\varphi + m_{BC}r^G_{BC}\cos(\varphi_{BC} + \psi_{BC})\partial_\varphi\varphi_{BC} + m_{CD}R_1\cos\varphi_{CD}\partial_\varphi\varphi_{CD}\\
B_{nl}(\varphi) &= m_{AB}R_0\sin\varphi + m_{CD}R_1\sin\varphi_{CD}\partial_\varphi\varphi_{CD} + m_{BC}[2R_0\sin\varphi + r^G_{BC}\sin(\varphi_{BC} + \psi_{BC})\partial_\varphi\varphi_{BC}]\\
K_{nl}(\varphi) &= -4kb^2\left\{\frac{1}{4}\sin\frac{\varphi_{BC}}{2}\partial_\varphi\varphi_{BC}\left[2 \mp \sin\left(\alpha \pm \varphi \pm \frac{\varphi_{BC}}{2}\right) \mp \sin\left(\alpha_1 \pm \varphi_{CD} \pm \frac{\varphi_{BC}}{2}\right)\right]\right.\\
&\quad \left. + \cos^2\frac{\varphi_{BC}}{4}\left[\cos\left(\alpha \pm \varphi \pm \frac{\varphi_{BC}}{2}\right)\left(1 + \frac{1}{2}\partial_\varphi\varphi_{BC}\right) + \cos\left(\alpha_1 \pm \varphi_{CD} \pm \frac{\varphi_{BC}}{2}\right)\left(\partial_\varphi\varphi_{CD} + \frac{1}{2}\partial_\varphi\varphi_{BC}\right)\right]\right\}\\
D_{nl}(\varphi) &= 2Cb^2\{[1 \pm \sin(\alpha \pm \varphi)] + [1 \pm \sin(\alpha \pm \varphi_{CD})]\partial_\varphi\varphi^2_{CD}\}
\end{aligned} \quad (18)$$

Owing to the lack of symmetry, the rocking mechanism differs depending on the sign of the rotation ϕ (Fig. 1), which is positive counterclockwise and negative clockwise. Note also that, for negative ϕ rotations, the distance $r_{BC,n}$ (measured from pivot point B to the center of mass G_{BC}) is larger, and the angle $\psi_{BC,n}$ is smaller than the corresponding distance $r_{BC,p}$ and angle $\psi_{BC,p}$ for positive ϕ rotations (Fig. 1). For this reason, depending on the sign of the rocking rotation, the following substitutions must be made in Eq. (18):

$$\begin{aligned}
&I_{BC} = I_{BC,p}, \quad r^G_{BC} = r^G_{BC,p}, \quad \psi_{BC} = \psi_{BC,p}, \quad \text{for } \phi = \varphi - \varphi_{0,p} > 0\\
&I_{BC} = I_{BC,n}, \quad r^G_{BC} = r^G_{BC,n}, \quad \psi_{BC} = \psi_{BC,n}, \quad \text{for } \phi = \varphi - \varphi_{0,n} < 0
\end{aligned} \quad (19)$$

Consequently, the minimum ground acceleration required to initiate rocking assumes different values for positive and negative rocking rotations. In either case, the minimum ground acceleration $\ddot{u}_{g,\min}$ capable of initiating rocking can be determined by substituting $\ddot{\varphi} = 0, \dot{\varphi} = 0, \phi = 0 \Rightarrow \varphi = \varphi_{0,p}, \varphi_{0,n}$ into Eq. (17):

$$\frac{\ddot{u}_{g,\min}}{g} = \frac{G_{nl}(0)}{B_{nl}(0)} = \lambda \quad (20)$$

Applying Eq. (20) for the two rocking mechanisms yields:

$$\lambda = \frac{\ddot{u}_{g,\min}}{g} = \mp\frac{b}{H}\frac{m_{AB} + m_{BC}[1 + \bar{h} - 2\bar{b}(\pm\bar{h} \mp 1)] + m_{CD}\bar{h}}{m_{AB} + 2m_{BC}[\frac{\bar{b}\bar{h}}{H}(\pm\bar{h} \mp 1) + 1] + m_{CD}} \quad (21)$$

where $\bar{h} = H/H_1$ = indicator of the asymmetry; and $\bar{b} = b/L$. Further, as a first approach, the study assumes the behavior of the supplemental tendons and dampers is elastic until brittle fracture (without previous yielding), which occurs simultaneously for all tendons and dampers. This is a simplifying assumption, the validity of which depends on the details of the particular case examined. Hence, if the tendons and the dampers reach the fracture elongation ε_f, say at time instant t_f, the equation of motion switches irreversibly to the equation of the freestanding frame [terms K_{nl} and D_{nl} in Eq. (17) disappear]. Note that both Eqs. (17) and (18) capture the motion of the symmetric hybrid frame as a special case ($H_1 = H$).

Equations of Impact and Contact

The equation of motion, Eq. (17), is valid for nonzero values of the rocking rotation ($\phi \neq 0$). When rocking rotation is zero $\phi = 0 \Rightarrow \varphi = \varphi_{0,p}$ or $\varphi = \varphi_{0,n}$, the frame is at the initial/rest position [Fig. 2(b)]. Let the preimpact rocking rotation be counterclockwise (positive) as in Fig. 2(a), and let impact occur at points A, B, C, and D [Fig. 2(b)].

To determine the postimpact state in the case of rocking, the impact problem of Fig. 2 needs to be solved. There are five unknowns: the impulses Λ_{Ax}, Λ_{Ay}, Λ_{Dx}, Λ_{Dy} at the corresponding pivot/impact points and the angular velocity after the impact $\dot{\varphi}^+$. In general, the impulse at point j Λ_j is defined as

$$\Lambda_j = \lim_{\Delta t_i \to 0}\int_{\Delta t_i} \lambda_j dt \quad (22)$$

where λ_j = pertinent impact force; and Δt_i = duration of the impact. All nonimpulsive forces (e.g., inertia forces and self-weights) are considered negligible compared with the impact forces. The following five equations are considered:

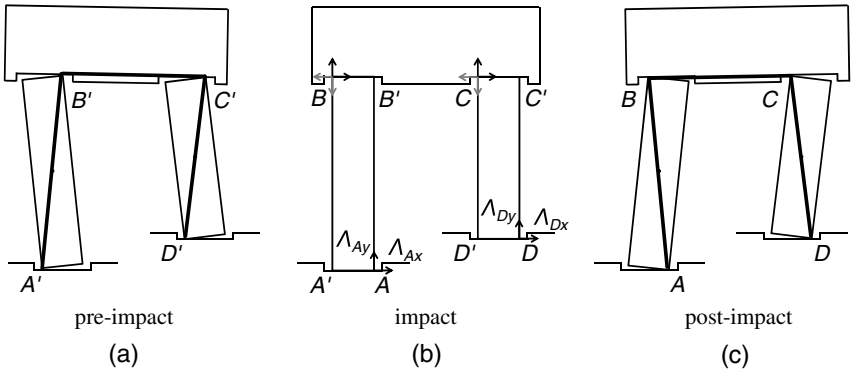

Fig. 2. Impulses Λ from (a) counterclockwise to (b) impact and (c) clockwise rotation

1. Linear momentum along x-axis for the whole frame

$$\Lambda_{Ax} + \Lambda_{Dx} = (m_{AB} + m_{CD} + 2m_{BC})H(\dot{\varphi}^- - \dot{\varphi}^+) - 2m_{BC}\bar{b}\bar{h}(1-\bar{h})(\dot{\varphi}^+ + \dot{\varphi}^-) \quad (23)$$

2. Linear momentum along y-axis for the whole frame

$$\Lambda_{Ay} + \Lambda_{Dy} = [-m_{AB}b - m_{CD}b\bar{h} - m_{BC}b(\bar{h}+1)](\dot{\varphi}^+ + \dot{\varphi}^-) - 2m_{BC}b\bar{b}(\bar{h}-1)(\dot{\varphi}^+ - \dot{\varphi}^-) \quad (24)$$

3. Moment of momentum about point A for the whole frame

$$L\Lambda_{Dy} - (2H - 2H_1)\Lambda_{Dx} = \left[I^G_{AB} + I^G_{CD}\bar{h} + m_{AB}H^2 + m_{CD}H(2H - H_1) + 2m_{BC}(2H + h)H - 2m_{BC} \times \left(\frac{L}{2} - b\right)b\bar{b}(\bar{h}-1)\right](\dot{\varphi}^+ - \dot{\varphi}^-) + \left[-I^G_{BC}2\bar{b}(\bar{h}-1) + m_{AB}b^2 - m_{CD}b\bar{h}(L-b) + 2m_{BC}(2H+h)\bar{b}\bar{h}(1-\bar{h}) - m_{BC}b\left(\frac{L}{2} - b\right)(1+\bar{h})\right](\dot{\varphi}^+ + \dot{\varphi}^-) \quad (25)$$

4. Moment of momentum about B for the left column of the frame

$$2H\Lambda_{Ax} + 2b\Lambda_{Ay} = (I^G_{AB} - m_{AB}H^2)(\dot{\varphi}^+ - \dot{\varphi}^-) - m_{AB}b^2(\dot{\varphi}^+ + \dot{\varphi}^-) \quad (26)$$

5. Moment of momentum about C for the right column of the frame

$$2H_1\Lambda_{Dx} + 2b\Lambda_{Dy} = (\bar{h}I^G_{CD} - m_{CD}HH_1)(\dot{\varphi}^+ - \dot{\varphi}^-) - m_{CD}b^2\bar{h}(\dot{\varphi}^+ + \dot{\varphi}^-) \quad (27)$$

where I^G_{AB}, I^G_{BC}, I^G_{CD} = moments of inertia of the frame members (AB, BC, CD) with respect to their center of mass. When the frame members are assumed as rigid blocks $I^G_{AB} = 1/3m_{AB}R_0^2$, $I^G_{CD} = 1/3m_{CD}R_1^2$, and $I^G_{BC} = m_{BC}\rho^2_{BC}$, where ρ_{BC} = polar radius of gyration. Eqs. (23)–(27) describe the impact problem for clockwise angular velocity. The impact problem for counterclockwise angular velocity is treated similarly, but the equations are not presented here for economy of space. The solution of the system of Eqs. (23)–(27) returns the four impulses and the postimpact angular velocity. The ratio of the angular velocities after and prior to the impact is defined as the coefficient of restitution $\eta = \dot{\varphi}^+/\dot{\varphi}^-$. In reality, the coefficient of restitution depends on many parameters that are usually (and herein) not simulated. Such parameters include but are not limited to the interface material and imperfections of the contact surface (ElGawady and Sha'lan 2011; Prieto et al. 2004). Therefore, the coefficient of restitution η should be considered as an independent parameter with problem-specific value. The solution of the system of Eqs. (23)–(27) provides solely a theoretical limit to the value of η needed to sustain pure rocking motion. Fig. 3 presents the coefficient of restitution (η) values for different column height ratios, and Appendix II offers the pertinent (general) closed-form expression for the coefficient of restitution.

For the symmetric rocking frame, the coefficient of restitution simplifies to:

$$\eta = \frac{\dot{\varphi}^+}{\dot{\varphi}^-} = \frac{1 - \frac{3}{2}\sin^2\alpha + 3\gamma\cos 2\alpha}{1 + 3\gamma} \quad (28)$$

where $\gamma = m_{BC}/2m_{AB}$, $\cos\alpha = H/R_0$, and $\sin\alpha = b/R_0$, thus verifying the result derived by Makris and Vassiliou (2012).

Recall that for the same asymmetric frame geometry, the rocking mechanism is different depending on the sign of the rocking rotation. In other words, similar to an asymmetric block, the asymmetric frame displays different slenderness depending on the sign of the rocking rotation ϕ, and accordingly varies the coefficient of restitution for clockwise and counterclockwise rotations (the two different curves of the frame geometry in Fig. 3).

Seismic Stability of the Asymmetric Rocking Frame

This section examines the seismic response of a planar asymmetric (freestanding and hybrid) rocking frame. Consider the rocking frame of Fig. 1. Assume a cap-beam 13 m wide with height $2h = 2$ m. The frame consists of two rectangular columns with $2b = 1.0$ m base length and width each, same density but different heights $2H = 7.0$ m and $2H_1 = 5.6$ m respectively, and the distance $L = 8$ m. The cap-beam/column mass ratio is taken as 10 according to Mander and Cheng (1997). The polar radius of gyration of the cap-beam cross section is assumed equal to 3.58 m, and the distances from the center of mass of the cap-beam to the two pivot points B and B′ are $r^G_{BC,n} = 4.64$ m and $r^G_{BC,p} = 3.68$ m (Fig. 1). For the hybrid frame, the damping and stiffness constants of the dampers and the tendons, accordingly, are assumed equal to 25.3 MNs/m and 23.5 MN/m following Mander and Cheng (1997). Finally, the cap-beam–column and the column–foundation connections prevent relative sliding, but allow uplifting and consequently act as simple/free supports.

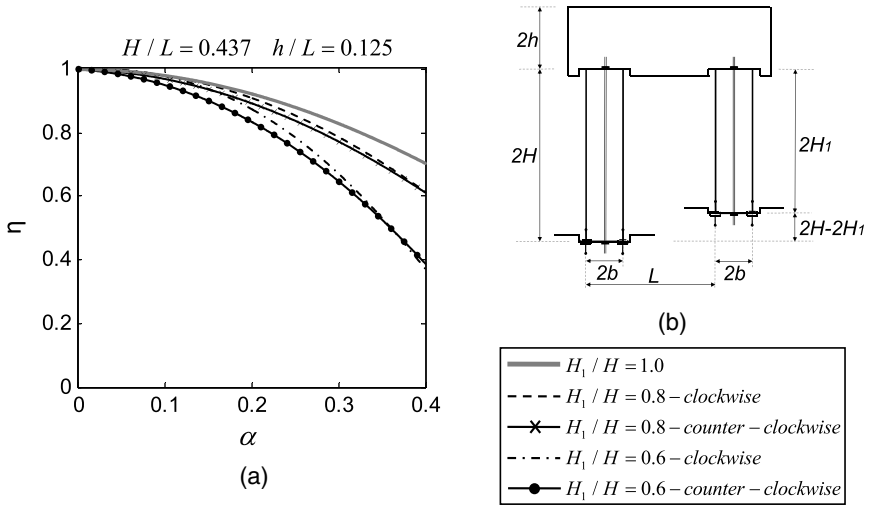

Fig. 3. (a) Coefficient of restitution of the (b) asymmetric rocking frame for different values of H_1/H; α = slenderness of the taller column (height $2H$); values used to create the figure are summarized in the section "Seismic Stability of the Asymmetric Rocking Frame"

Mathematical (Pulse-Type) Ground Motions

Large rocking structures (e.g., a rocking bridge bent) are more vulnerable to low-frequency coherent ground motions [e.g., Acikgoz and DeJong (2014) and references therein]. Therefore, to assess the seismic stability of the rocking frame, the study first considers pulse-type excitations. Acceleration or velocity pulses often characterize strong ground motions near the fault of major earthquakes and represent their most destructive (from a structural point of view) component (Dimitrakopoulos et al. 2009). Various mathematical pulses have been proposed in the literature that can capture the long-distinct pulses of near-fault ground motions both qualitatively and quantitatively (Acikgoz and DeJong 2014; Kafle et al. 2011; Voyagaki et al. 2013).

Herein, the Ricker pulse (Ricker 1943, 1944) is considered. The Ricker pulse can be defined with two parameters: the acceleration

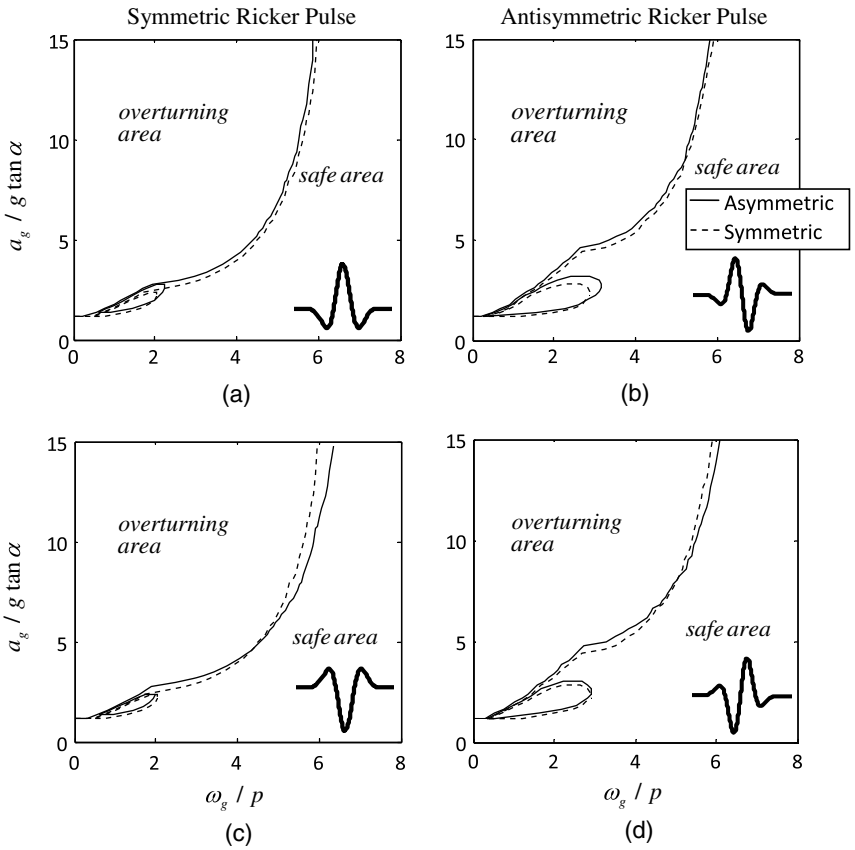

Fig. 4. Overturning plots of the symmetric and asymmetric freestanding rocking frame, under positive (a) symmetric, (b) antisymmetric; and negative (c) symmetric, (d) antisymmetric sign of Ricker pulse excitations

(a_g) or the velocity (v_g) amplitude, and the period T_g. Eq. (29) describes the symmetric Ricker pulse (Mexican hat wavelet)

$$\ddot{u}_g(t) = a_g\left(1 - \frac{2\pi^2 t^2}{T_g^2}\right)\exp\left(-\frac{1}{2}\frac{2\pi^2 t^2}{T_g^2}\right) \tag{29}$$

Similarly, Eq. (30) is known as the antisymmetric Ricker pulse (Vassiliou and Makris 2011)

$$\ddot{u}_g(t) = \frac{a_g}{\beta}\left(\frac{4\pi^2 t^2}{3T_g^2} - 3\right)\frac{2\pi t}{\sqrt{3}T_g}\exp\left(-\frac{1}{2}\frac{4\pi^2 t^2}{3T_g^2}\right) \tag{30}$$

In both cases [Eqs. (29) and (30)] the value of $T_g = 2\pi/\omega_g$ is the period that maximizes the Fourier spectrum of the corresponding Ricker wavelet. In Eq. (30), $\beta = 1.38$ enforces the function to have a maximum equal to the acceleration amplitude a_g.

The consideration of pulse-type excitations also facilitates the use of dimensionless variables (DeJong and Dimitrakopoulos 2014; Dimitrakopoulos and DeJong 2012b) which, if appropriately selected (Dimitrakopoulos and DeJong 2012b), offer a physically similar description of the response. A detailed discussion of the self-similar description of the rocking response is beyond the scope of the present work; therefore, the interested reader is referred to Dimitrakopoulos and DeJong (2012b). For the needs of the present analysis, the following results are scaled simply with respect to the rocking properties (frequency parameter $p = \sqrt{3g/4R_0}$ and slenderness α) of the highest column (height $2H$) of the frame as in Makris and Vassiliou (2012).

The overturning plot [e.g., Fig. 4(a)] separates the control plane ($\alpha_g/g\tan\alpha - \omega_p/p$) into two areas, one where the structure overturns (after impact or without any preceding impact) and one safe (no overturning) area. Recall that rocking structures exhibit various overturning modes with respect to the preceding impacts (Fielder et al. 1997). Fig. 4 shows that the structure is most vulnerable for low-frequency acceleration pulses, although it survives even high amplitude higher-frequency pulses. Thus, the seismic stability of the rocking frame under pulse-type excitations is typical of rocking systems (Dimitrakopoulos and DeJong 2012b), and in that sense, predictable. Interestingly, the effect of the asymmetry on the overall seismic stability of the rocking frame is marginal. Fig. 4 compares the stability of a symmetric and an asymmetric rocking frame that are both freestanding and subjected to the same Ricker pulses. The columns of the asymmetric frame are of unequal height ($H_1/H = 0.8$), but this asymmetry is almost immaterial to the overall stability of the frame. This is true regardless of the very different kinematics the asymmetric frame exhibits during its rocking response (i.e., the rigid body rotation of the cap-beam). Note that because of the lack of symmetry, both signs of each Ricker (symmetric and antisymmetric) pulse excitations are examined. However, the differentiation of the response for pulse excitations of opposite signs (e.g., the top versus bottom plots from Figs. 4 to 7) is consistently minor; nevertheless, as the asymmetry grows, the stability of the frame marginally decreases. In short, Fig. 4 suggests that compared with inherent uncertainties of seismic engineering, e.g. with regard to the earthquake loading prediction or the simplifications of the proposed analysis, the effect of the different rocking kinematics due to the unequal columns is not alarming for typical

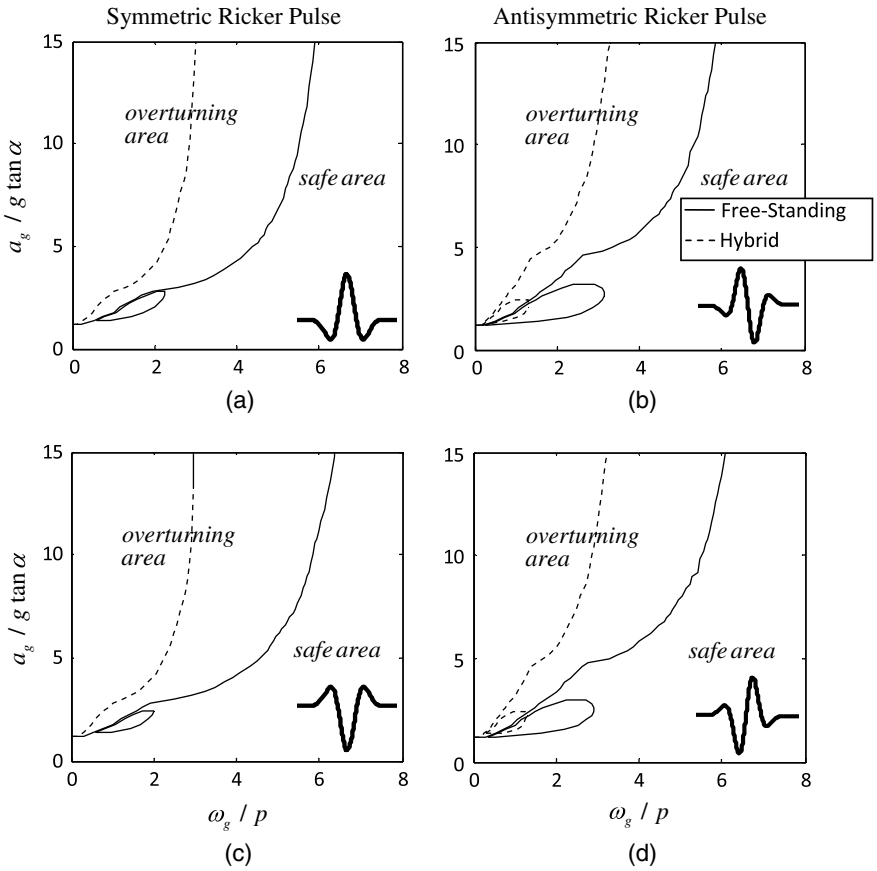

Fig. 5. Overturning plots of the asymmetric, freestanding, and hybrid rocking frame considering no fracture, under positive (a) symmetric, (b) antisymmetric; and negative (c) symmetric, (d) antisymmetric sign of Ricker pulse excitations

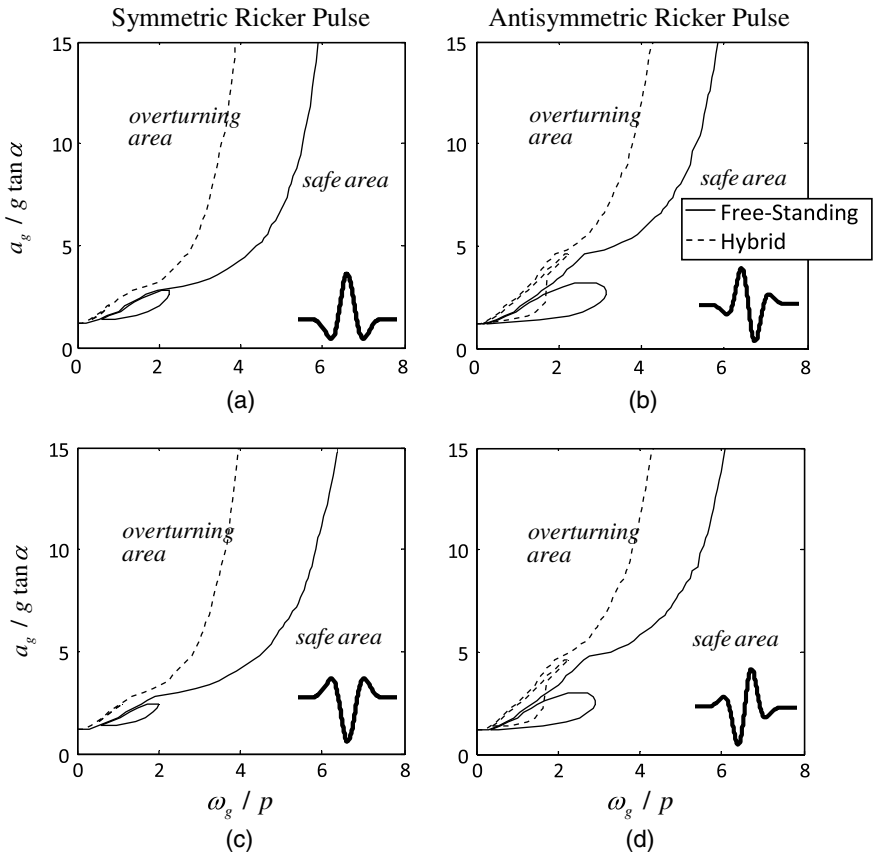

Fig. 6. Overturning plots of the asymmetric, freestanding, and hybrid rocking frame for 2.0% fracture elongation under positive (a) symmetric, (b) antisymmetric; and negative (c) symmetric, (d) antisymmetric sign of Ricker pulse excitations

geometries of rocking frames. Note that $H_1/H = 0.8$ is a probably high value intentionally selected to cover even extreme cases.

To limit the amplitude of rocking rotations and enhance the seismic stability of the rocking frame, this study investigates the use of unbonded (slack) central tendons and external viscous dampers (Fig. 1); converting the freestanding frame into a hybrid rocking frame. As a first approach, both tendons and dampers are assumed linear-elastic until their simultaneous brittle failure at fracture elongation ε_f. However, an indication of the effects of a ductile tendon behavior can be found in Makris and Zhang (2001). Before the freestanding frame overturns, it must first achieve extensive rocking rotations. The exact critical rocking rotation, beyond which the structure becomes unstable, is given by the solution of the nonlinear equation $\partial_\varphi V = 0$. As an order of magnitude, however, and in the case of slack tendons, the critical rotation is of the same order as the slenderness $\phi_{cr} = \alpha$, whereas for stiffer tendons, the critical rotation increases. Consequently, rotations of the hybrid frame near overturning correspond roughly to elongations of the tendon in the order of 2.0% [assuming a tendon length equal to 8.5 m as in Mander and Cheng (1997)]. In other words, the critical fracture rotation of the frame is $\phi_f = \varepsilon_f l/2b$. Figs. 5–7 present the seismic stability of the hybrid and freestanding (same asymmetric geometry) rocking frames for different fracture elongations. In particular, in Fig. 5, ε_f is high enough to ensure the system of tendons and dampers stays within the linear-elastic range until overturning, whereas in Figs. 6 and 7, the fracture elongation is taken as $\varepsilon_f =$ 2.0 and 1.0% respectively. The comparison of Figs. 5–7 unveils the sensitivity of the seismic performance/stability of the rocking frame to the assumed fracture elongation (the only difference between Figs. 5 to 7). In general, the higher the fracture elongation, the more drastic the enhancement of the stability is.

Interestingly, however, the response of the hybrid frame is not always better compared with the freestanding frame. Neither is the stability always enhanced the higher the fracture elongation becomes. Similar to the anchored rocking block (Dimitrakopoulos and DeJong 2012a), countertrends also appear where the response of the hybrid frame is worse than that of the corresponding freestanding frame. Figs. 4 and 7 illustrate such combinations, wherein the hybrid frame overturns when the freestanding frame survives the excitation; for instance, when $\alpha_g/g\tan\alpha \approx 3 \div 4$, $\omega_p/p \approx 2 \div 3$, and the excitation is an antisymmetric Ricker pulse (Fig. 7). These peculiar response characteristics stem from the frail (highly nonlinear) nature of rocking dynamics, and in that sense are anticipated.

Historic Excitations

The present section extends the seismic stability analysis of the same asymmetric rocking frame, examining historic excitations regardless of whether they contain distinguishable pulses or not. In particular, a well-known set of historic ground motions scaled to yield a probability of exceedance of 2% in 50 years (SAC 1997) is examined.

Figs. 8 and 9 compare the response of the freestanding and the hybrid asymmetric rocking frame, in terms of time-history and peak response, respectively. For the hybrid frame, a fracture elongation of $\varepsilon_f = 1.0\%$ is assumed. Although the examined ground motions are scaled to the maximum credible earthquake level,

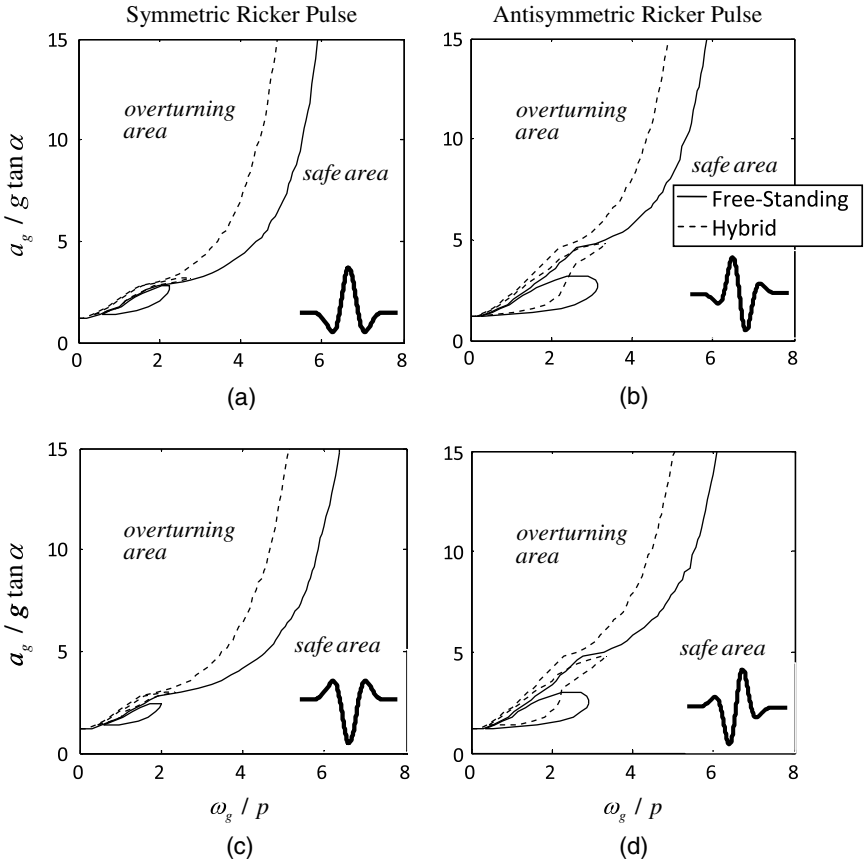

Fig. 7. Overturning plots of the asymmetric, freestanding, and hybrid, rocking frame for 1.0% fracture elongation under positive (a) symmetric, (b) antisymmetric; and negative (c) symmetric, (d) antisymmetric sign of Ricker pulse excitations

the freestanding rocking frame survives most of them, and the pertinent hybrid frame survives all ground motions listed in Table 1. Recall that according to the assumptions of the present analysis, when the structure survives the motion (i.e., does not overturn), it eventually re-centers, and hence there is no permanent rotation and/or expected damage, which is the premise of the *damage-avoidance design* (Mander and Cheng 1997).

Interestingly, the most destructive among the historic records examined are SE23, SE24 from the 1992 Erzican, Turkey earthquake. Again, this is due to the distinguishable dominant impulsive motions these records contain.

On the other hand, although the hybrid rocking frame survives all excitations examined herein (Fig. 9), it is precarious to derive general conclusions for other excitations. This is particularly true for noncoherent seismic excitations because the rocking response becomes less orderly (Acikgoz and DeJong 2014). Therefore, a more general answer regarding the seismic reliability of rocking behavior/structures to noncoherent excitations should be couched

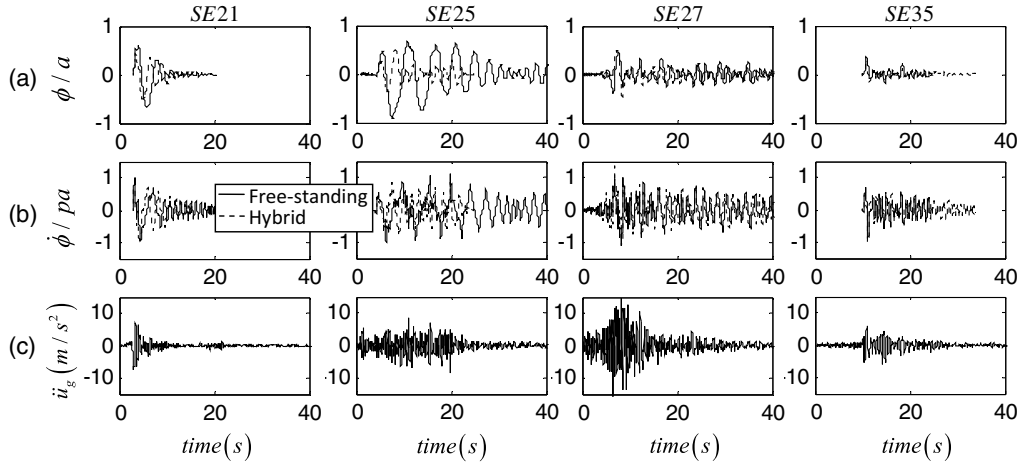

Fig. 8. Seismic response of an asymmetric rocking frame: (a) dimensionless rocking rotation; and (b) dimensionless angular velocity for (c) different earthquake records

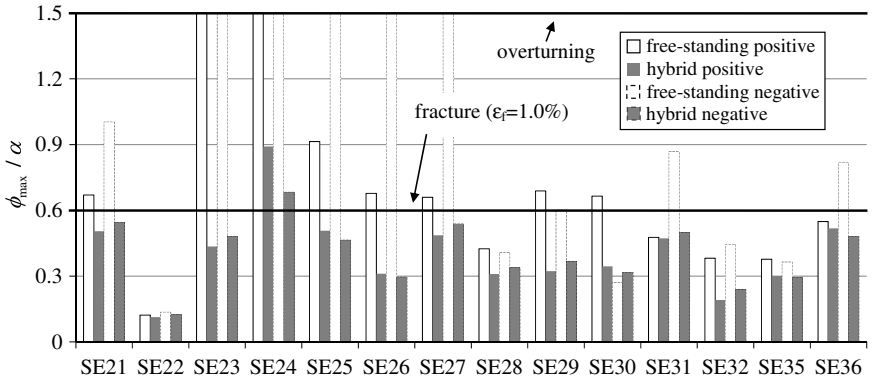

Fig. 9. Maximum rotations (in dimensionless terms) for all the earthquake records of Table 1 for both directions of the excitation (positive and negative)

Table 1. Earthquake Records (Probability of Exceedance of 2% in 50 Years) (Data from SAC 1997)

Number	Record	Magnitude	Scale factor	DT (s)	Duration (s)	PGA (cm/s^2)
SE21	1992 Mendocino	7.1	0.98	0.02	59.98	741.13
SE22	1992 Mendocino	7.1	0.98	0.02	59.98	476.22
SE23	1992 Erzincan	6.7	1.27	0.005	20.775	593.60
SE24	1992 Erzincan	6.7	1.27	0.005	20.775	529.06
SE25	1949 Olympia	6.5	4.35	0.02	79.98	878.23
SE26	1949 Olympia	6.5	4.35	0.02	79.98	805.68
SE27	1965 Seattle	7.1	10.04	0.02	81.82	1,722.40
SE28	1965 Seattle	7.1	10.04	0.02	81.82	1,364.70
SE29	1985 Valparaiso	8.0	2.9	0.025	99.975	1,605.50
SE30	1985 Valparaiso	8.0	2.9	0.025	99.975	1,543.50
SE31	1985 Valparaiso	8.0	3.96	0.025	99.975	1,246.20
SE32	1985 Valparaiso	8.0	3.96	0.025	99.975	884.43
SE35	1978 Miyagi-oki	7.4	1.78	0.02	79.98	595.07
SE36	1978 Miyagi-oki	7.4	1.78	0.02	79.98	768.62

in probabilistic methods. This task, however, is beyond the scope of the present paper.

Conclusions

This study investigates the seismic response of a planar rocking frame as a potential (alternative) seismic design paradigm. Treating the structure as a generalized single-degree-of-freedom system, it formulates the equations of motion, and sheds light on the impact mechanism.

In particular, the paper examines the case of asymmetric frame geometry (columns of unequal height) and compares the seismic stability of the freestanding with the hybrid (supplemented with additional restoring and damping capacity) rocking frame. Both mathematical pulse-type ground motions as well as historic earthquake records are examined.

The analysis shows that despite the very different kinematics of the symmetric and the asymmetric frame geometry, the overall stability under pulse-type excitations is unaffected, at least for the geometries examined. This counterintuitive finding is reassuring regarding the potential merits of the rocking frame as a high-performance design solution. The results also unveil the dominant role of the fracture elongation of the, assumed elastic-brittle, supplemental tendons and dampers, on the behavior of the hybrid frame. The seismic stability is sensitive to the fracture elongation and, in general, the higher the fracture elongation, the more drastic the improvement of the seismic performance of the rocking frame.

Finally, the study shows that the hybrid frame would survive all historic earthquake excitations examined, even though they are scaled to the maximum credible earthquake level. Thus, the paper confirms the ample seismic stability of the (planar) hybrid rocking frame, and verifies its promising high-performance seismic behavior.

Appendix I. Strain Energy Expression

Appendix I provides the strain energy expression due to the elongation of the tendons for both large and small rotations. Considering the definition of the rocking rotations ϕ, and ϕ_1 [Eq. (12)], the strain energy of the tendons [Eq. (9)] can be written as

$$V_{\text{tend}} = 4kb^2\left(\cos^2\frac{\varphi_{\text{BC}}}{4}\right)\left[2\mp\sin\left(\alpha\pm\varphi\pm\frac{\varphi_{\text{BC}}}{2}\right)\mp\sin\left(\alpha_1\pm\varphi_{\text{CD}}\pm\frac{\varphi_{\text{BC}}}{2}\right)\right] \tag{31}$$

For small rotations the tendon elongation expressions simplify to

$$\delta l_{\text{A}} = \delta l_{\text{B}} = b\phi \tag{32}$$

and

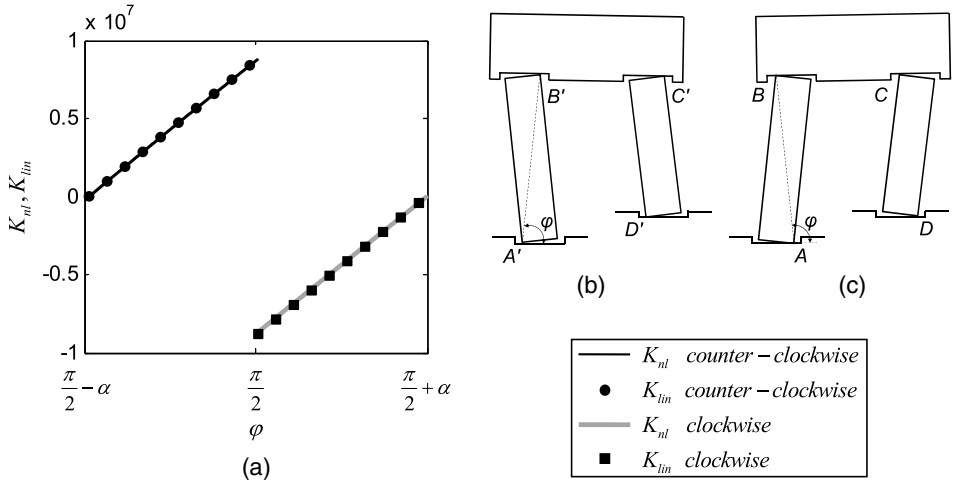

Fig. 10. (a) Comparison of the nonlinear term K_{nl} [Eq. (18)] with the linearized K_{lin} [Eq. (35)] in terms of the angle φ, for (b) counterclockwise and (c) clockwise rotation; values used to create the figure are summarized in the section "Seismic Stability of the Asymmetric Rocking Frame"

$$\delta l_{\text{D}} = \delta l_{\text{C}} = b\phi_1 \tag{33}$$

For the cases considered in this paper, the small rotations assumption offers a dependable approximation (Fig. 10) of the stiffness

$$V_{\text{tend(lin)}} = 2kb^2(1+\bar{h}^2)\left(-\frac{\pi}{2} \pm \alpha + \varphi\right)^2 \tag{34}$$

In Fig. 10, K_{lin} is the partial derivative of the strain energy with respect to the angle φ

$$K_{\text{lin}} = \partial V_{\text{tend(lin)}}/\partial\varphi = 4kb^2(1+\bar{h}^2)\left(-\frac{\pi}{2} \pm \alpha + \varphi\right) \tag{35}$$

Appendix II. General Closed-Form Expression for the Coefficient of Restitution of the Asymmetric Rocking Frame

This appendix offers the general closed-form expression for the coefficient of restitution of the asymmetric rocking frame. In particular, the coefficient of restitution η is calculated by the solution of the system of Eqs. (23)–(27) as

$$\eta = \frac{\{[2\bar{b}(\bar{h}-1)\mp 1](\pm a_1 + a_2 - a_3 \mp a_4) \pm \bar{b}(\bar{h}-1)\times(a_6 - a_5) + [\pm\bar{b}(\bar{h}-1) - \frac{1}{2}](a_7 + a_8) + [\bar{b}(\bar{h}-1)\mp\frac{1}{2}\bar{h}](a_9 + a_{10})\}}{\{[2\bar{b}(\bar{h}-1)\mp 1](\pm a_1 - a_2 + a_3 \mp a_4) \pm \bar{b}(1-\bar{h})\times(a_5 + a_6) + [\pm\bar{b}(\bar{h}-1) - \frac{1}{2}](a_7 - a_8) \pm [\bar{b}(\bar{h}-1)\mp\frac{1}{2}\bar{h}](a_9 - a_{10})\}} \tag{36}$$

where

$$a_1 = (m_{\text{AB}} + m_{\text{CD}} + 2m_{\text{BC}})H^2 \qquad a_2 = 2m_{\text{BC}}\bar{b}(1-\bar{h})Hh \qquad a_3 = \pm m_{\text{AB}}b^2 \pm m_{\text{CD}}b^2\bar{h} \pm m_{\text{BC}}b^2(1+\bar{h})$$

$$a_4 = 2m_{\text{BC}}b^2\bar{b}(\bar{h}-1) \qquad a_5 = \left[I^G_{\text{AB}} + I^G_{\text{CD}}\bar{h} + m_{\text{AB}}H^2 + m_{\text{CD}}H(2H - H_1) + 2m_{\text{BC}}H(2H+h) - 2m_{\text{BC}}b\bar{b}\left(\frac{L}{2} \pm b\right)(\bar{h}-1)\right]$$

$$a_6 = \left[\pm I^G_{\text{BC}}2\bar{b}(\bar{h}-1) + m_{\text{AB}}b^2 \pm m_{\text{CD}}b\bar{h}(L \pm b) \mp 2m_{\text{BC}}\bar{b}h(2H+h)(1-\bar{h}) \pm m_{\text{BC}}b\left(\frac{L}{2} \pm b\right)(\bar{h}+1)\right] \qquad a_7 = I^G_{\text{AB}} - m_{\text{AB}}H^2$$

$$a_8 = m_{\text{AB}}b^2 \qquad a_9 = \bar{h}I^G_{\text{CD}} - m_{\text{CD}}HH_1 \qquad a_{10} = m_{\text{CD}}b^2\bar{h} \qquad \bar{h} = \frac{H}{H_1} \qquad \bar{b} = \frac{b}{L} \tag{37}$$

Again, in Eqs. (31)–(37), the upper sign denotes the counterclockwise (positive) rotation, and the lower sign the clockwise (negative) rotation.

Acknowledgments

Financial support was provided by the Research Grants Council of Hong Kong, under grant reference number ECS 639613. Discussions with Lecturer Matthew DeJong of the University of Cambridge are also gratefully acknowledged.

References

Aaleti, S., and Sritharan, S. (2009). "A simplified analysis method for characterizing unbonded post-tensioned precast wall systems." *Eng. Struct.*, 31(12), 2966–2975.

Acikgoz, S., and DeJong, M. J. (2014). "The rocking response of large flexible structures to earthquakes." *Bull. Earthquake Eng.*, 12(2), 875–908.
Antonellis, G., and Panagiotou, M. (2013). "Seismic response of bridges with rocking foundations compared to fixed-base bridges at a near-fault site." *J. Bridge Eng.*, 10.1061/(ASCE)BE.1943-5592.0000570, 04014007.
Brogliato, B., Zhang, H., and Liu, C. (2012). "Analysis of a generalized kinematic impact law for multibody-multicontact systems, with application to the planar rocking block and chains of balls." *Multibody Syst. Dyn.*, 27(3), 351–382.
Ceccarelli, M. (2007). *Distinguished figures in mechanism and machine science: Their contributions and legacies*, Springer, Netherlands.
Chatzis, M., and Smyth, A. (2012). "Modeling of the 3D rocking problem." *Int. J. Non Linear Mech.*, 47(4), 85–98.
Chen, Y. H., Liao, W. H., Lee, C. L., and Wang, Y. P. (2006). "Seismic isolation of viaduct piers by means of a rocking mechanism." *Earthquake Eng. Struct. Dyn.*, 35(6), 713–736.
Cheng, C.-T. (2008). "Shaking table tests of a self-centering designed bridge substructure." *Eng. Struct.*, 30(12), 3426–3433.
DeJong, M. J., and Dimitrakopoulos, E. G. (2014). "Dynamically equivalent rocking structures." *Earthquake Eng. Struct. Dyn.*, 43(10), 1543–1563.
Dimitrakopoulos, E., Kappos, A. J., and Makris, N. (2009). "Dimensional analysis of yielding and pounding structures for records without distinct pulses." *Soil Dyn. Earthquake Eng.*, 29(7), 1170–1180.
Dimitrakopoulos, E. G., and DeJong, M. J. (2012a). "Overturning of retrofitted rocking structures under pulse-type excitations." *J. Eng. Mech.*, 10.1061/(ASCE)EM.1943-7889.0000410, 963–972.
Dimitrakopoulos, E. G., and DeJong, M. J. (2012b). "Revisiting the rocking block: Closed-form solutions and similarity laws." *Proc. R. Soc. London, Ser. A*, 468(2144), 2294–2318.
Dimitrakopoulos, E. G., and DeJong, M. J. (2013). "Seismic overturning of rocking structures with external viscous dampers." *Computational methods in earthquake engineering*, Manolis Papadrakakis, Michalis Fragiadakis, and Vagelis Plevris, eds., Springer, Greece, 243–258.
Dimitrakopoulos, E. G., DeJong, M. J., and Giouvanidis, A. I. (2013). "Seismic assessment of rocking bridge bents using an equivalent rocking block." *2013 World Congress on Advances in Structural Engineering and Mechanics (Session T4I-I)*, Korea Federation of Science and Technology Societies, International Association of Structural Engineering & Mechanics (IASEM), Korea National Tourism Corporation, Jeju Convention & Visitors Bureau, Jeju, Korea.
Eatherton, M. R., et al. (2014). "Design concepts for controlled rocking of self-centering steel-braced frames." *J. Struct. Eng.*, 10.1061/(ASCE)ST.1943-541X.0001047, 04014082.
ElGawady, M. A., and Sha'lan, A. (2011). "Seismic behavior of self-centering precast segmental bridge bents." *J. Bridge Eng.*, 10.1061/(ASCE)BE.1943-5592.0000174, 328–339.
Fielder, W., Virgin, L., and Plaut, R. (1997). "Experiments and simulation of overturning of an asymmetric rocking block on an oscillating foundation." *Eur. J. Mech. A. Solids*, 16(5), 905–923.
Freudenstein, F. (2010). "Approximate synthesis of four-bar linkages." *Resonance*, 15(8), 740–767.
Housner, G. W. (1963). "The behavior of inverted pendulum structures during earthquakes." *Bull. Seismol. Soc. Am.*, 53(2), 403–417.
Kafle, B., Lam, N. T., Gad, E. F., and Wilson, J. (2011). "Displacement controlled rocking behaviour of rigid objects." *Earthquake Eng. Struct. Dyn.*, 40(15), 1653–1669.
Kam, W. Y., Pampanin, S., Palermo, A., and Carr, A. J. (2010). "Self-centering structural systems with combination of hysteretic and viscous energy dissipations." *Earthquake Eng. Struct. Dyn.*, 39(10), 1083–1108.
Kelly, J. M., and Tsztoo, D. (1977). "Earthquake simulation testing of a stepping frame with energy-absorbing devices." *Bull. N. Z. Natl. Soc. Earthquake Eng.*, 10(4), 196–207.
Makris, N., and Vassiliou, M. F. (2012). "Planar rocking response and stability analysis of an array of free-standing columns capped with a freely supported rigid beam." *Earthquake Eng. Struct. Dyn.*, 42(3), 431–449.
Makris, N., and Vassiliou, M. F. (2014). "Are some top-heavy structures more stable?" *J. Struct. Eng.*, 10.1061/(ASCE)ST.1943-541X.0000933, 06014001.
Makris, N., and Zhang, J. (2001). "Rocking response of anchored blocks under pulse-type motions." *J. Eng. Mech.*, 10.1061/(ASCE)0733-9399(2001)127:5(484), 484–493.
Mander, J. B., and Cheng, C.-T. (1997). "Seismic resistance of bridge piers based on damage avoidance design." *Technical Rep.*, National Center for Earthquake Engineering Research, State Univ. of New York, Buffalo, New York.
Marriott, D., Pampanin, S., and Palermo, A. (2009). "Quasi-static and pseudo-dynamic testing of unbonded post-tensioned rocking bridge piers with external replaceable dissipaters." *Earthquake Eng. Struct. Dyn.*, 38(3), 331–354.
Oppenheim, I. J. (1992). "The masonry arch as a four-link mechanism under base motion." *Earthquake Eng. Struct. Dyn.*, 21(11), 1005–1017.
Palermo, A., Pampanin, S., and Calvi, G. M. (2005). "Concept and development of hybrid solutions for seismic resistant bridge systems." *J. Earthquake Eng.*, 9(6), 899–921.
Palermo, A., Pampanin, S., and Marriott, D. (2007). "Design, modeling, and experimental response of seismic resistant bridge piers with post-tensioned dissipating connections." *J. Struct. Eng.*, 10.1061/(ASCE)0733-9445(2007)133:11(1648), 1648–1661.
Pang, J. B., Stanton, J. F., and Eberhard, M. O. (2008). "A precast concrete bridge bent designed to re-center after an earthquake." *Research Rep.*, Washington State Transportation Center, Univ. of Washington, Seattle, Washington.
Papaloizou, L., and Komodromos, P. (2009). "Planar investigation of the seismic response of ancient columns and colonnades with epistyles using a custom-made software." *Soil Dyn. Earthquake Eng.*, 29(11), 1437–1454.
Papaloizou, L., and Komodromos, P. (2012). "Investigating the seismic response of ancient multi-drum colonnades with two rows of columns using an object-oriented designed software." *Adv. Eng. Software*, 44(1), 136–149.
Pollino, M., and Bruneau, M. (2007). "Seismic retrofit of bridge steel truss piers using a controlled rocking approach." *J. Bridge Eng.*, 10.1061/(ASCE)1084-0702(2007)12:5(600), 600–610.
Priestley, M. N., Seible, F., and Calvi, G. M. (1996). *Seismic design and retrofit of bridges*, Wiley, New York.
Priestley, M. N., and Tao, J. R. (1993). "Seismic response of precast prestressed concrete frames with partially debonded tendons." *PCI J.*, 38(1), 58–69.
Prieto, F., Lourenço, P. B., and Oliveira, C. (2004). "Impulsive Dirac-delta forces in the rocking motion." *Earthquake Eng. Struct. Dyn.*, 33(7), 839–857.
Psycharis, I. N., Fragiadakis, M., and Stefanou, I. (2013). "Seismic reliability assessment of classical columns subjected to near-fault ground motions." *Earthquake Eng. Struct. Dyn.*, 42(14), 2061–2079.
Ricker, N. (1943). "Further developments in the wavelet theory of seismogram structure." *Bull. Seismol. Soc. Am.*, 33(3), 197–228.
Ricker, N. (1944). "Wavelet functions and their polynomials." *Geophysics*, 9(3), 314–323.
Roh, H., and Reinhorn, A. M. (2010). "Modeling and seismic response of structures with concrete rocking columns and viscous dampers." *Eng. Struct.*, 32(8), 2096–2107.
Sakai, J., and Mahin, S. A. (2004). "Mitigation of residual displacements of circular reinforced concrete bridge columns." *Proc., 13th World Conf. on Earthquake Engineering*, Vancouver, Canada.
Skinner, R., Tyler, R., Heine, A., and Robinson, W. (1980). "Hysteretic dampers for the protection of structures from earthquakes." *Bull. N. Z. Natl. Soc. Earthquake Eng.*, 13(1), 22–36.
Solberg, K., Mashiko, N., Mander, J., and Dhakal, R. (2009). "Performance of a damage-protected highway bridge pier subjected to bidirectional earthquake attack." *J. Struct. Eng.*, 10.1061/(ASCE)0733-9445(2009)135:5(469), 469–478.
Structural Engineers Association of California (SEA), Applied Technology Council (ATC) and Consortium of Universities for Research in Earthquake Engineering (CUREE). (1997). "Suites of earthquake ground motions." ⟨http://nisee.berkeley.edu/data/strong_motion/sacsteel/ground_motions.html⟩ (Jan. 10, 2014).

Vassiliou, M. F., and Makris, N. (2011). "Estimating time scales and length scales in pulselike earthquake acceleration records with wavelet analysis." *Bull. Seismol. Soc. Am.*, 101(2), 596–618.

Voyagaki, E., Psycharis, I. N., and Mylonakis, G. (2013). "Rocking response and overturning criteria for free standing rigid blocks to single—lobe pulses." *Soil Dyn. Earthquake Eng.*, 46, 85–95.

Wacker, J. M., Hieber, D. G., Stanton, J. F., and Eberhard, M. O. (2005). "Design of precast concrete piers for rapid bridge construction in seismic regions." *Research Rep.*, Washington State Transportation Center, Univ. of Washington, Seattle, Washington.

Zulli, D., Contento, A., and Di Egidio, A. (2012). "3D model of rigid block with a rectangular base subject to pulse-type excitation." *Int. J. Non Linear Mech.*, 47(6), 679–687.